A Prototype Modular Detector Design for High Resolution Positron Emission Mammography Imaging

Nan Zhang, *Member, IEEE*, Christopher J. Thompson, *Member, IEEE*, Francois Cayouette, *Member, IEEE*, Dean Jolly, and Steve Kecani

Abstract—Current challenges facing us in developing dedicated position emission tomography (PET) system for metabolic breast mammography (PEM) and small animal (ANIPET) are to achieve high spatial resolution (less than 2 mm) and high efficiency. It is also crucial to extend the sensitive areas of PEM detectors to their periphery in order to overcome the difficulty in imaging near a patient's chest wall. This limitation of the periphery dead region was revealed in the clinical trials of our previously developed PEM-I system.

In the new study, we developed prototype detectors by using position-sensitive photomultiplier tubes (PS-PMTs) and pixelated bismuth germanate (BGO) crystals with depth encoding scheme to detect and localize gamma rays. The procedures in crystal processing include cutting, polishing, encapsulating, separating, and re-gluing. We also developed front-end electronic circuits including high-voltage dividers, anode resistor chains, position readout circuits, and last dynode timing circuits. Methods for combining four PS-PMTs with simple $X+$, $X-$, $Y+$, $Y-$ outputs have been developed to further simplify the position recording. The detectors were constructed in the structure of array (two in the system)—module (four in each array)—unit (four in each module). The basic unit of one crystal and one PS-PMT can be field replaceable.

Our new prototype detectors show that the proposed PEM-II system has a spatial resolution of 1.8 mm (versus 2.8 mm in PEM-I), a timing resolution of 10.3 ns (versus 12 ns in PEM-I), and a field-of-view of 88 mm $\times$ 88 mm (versus 64 mm $\times$ 56 mm in PEM-I). Compared with our previous PEM-I system, it demonstrates that the design improves the spatial resolution, enhances the detector field-of-view, and significantly reduces the peripheral dead regions.

Index Terms—Bismuth germanate (BGO) crystal, position-sensitive photomultiplier tube (PS-PMT), positron emission mammography (PEM), positron emission tomography (PET).

N. Zhang was with the Biomedical Engineering Department and the Montreal Neurological Institute, McGill University, Montreal, QC H3A2B4, Canada. He is now with CPS Innovations, Inc., Rockford, TN 37853 USA (e-mail: nan.zhang@cpspet.com).

C. J. Thompson and F. Cayouette are with the Biomedical Engineering Department and the Montreal Neurological Institute, McGill University, Montreal, QC H3A2B4, Canada (e-mail: christopher.thompson@mcgill.ca; francois.cayouette@mail.mcgill.ca).

D. Jolly is with the Medical Cyclotron Facility of the Montreal Neurological Institute, McGill University, Montreal, QC H3A2B4, Canada (e-mail: deanj@bic.mni.mcgill.ca).

S. Kecani is with the Machine Shop, Physics Department, McGill University, Montreal, QC H3A2T8, Canada (e-mail: kecani@physics.mcgill.ca).

I. INTRODUCTION

DEDICATED PET instruments for small animal (ANIPET system) and breast imaging (PEM-I) were previously developed in our lab of the Montreal Neurological Institute, McGill University [1]–[3]. Each system consists of two detectors; each detector is constructed with four 36 mm $\times$ 36 mm $\times$ 20 mm Bismuth germanate (BGO) crystal blocks optically coupled to a Hamamatsu R3941-05 PS-PMT [4]. Electronic circuits in these detectors consist of high voltage dividers, crossed anode read-out resistor chains, position preamplifiers, and fast timing amplifier circuits. The system spatial resolution is 2.8 mm; the timing resolution is 12 ns. The detector field-of-view is 64 mm $\times$ 56 mm [5].

Our clinical studies with PEM-I system revealed that the detectors have relatively large peripheral dead regions. This is mainly caused by the PMT intrinsic structure. R3941 is a mesh type PS-PMT with a thick glass envelop. The PMT light-photon input window is in a photocathode head-on configuration. The cross-anode outputs have 18 anodes in the X-axis and 16 anodes in the Y-axis. Even though the outer dimension of the PMT is 78 mm $\times$ 78 mm, its effective input window, or the effective field-of-view, is only about 60 mm $\times$ 54 mm [4]. In the detectors of PEM-I and ANIPET, BGO crystals cover the PMT window in a region of 72 mm $\times$ 72 mm. After the previous efforts to develop and improve readout weighting matrix for the PMT, we identified crystal elements in the area of 64 mm $\times$ 56 mm [5], [6]. However, there are still 7-mm periphery dead regions in each end of X-axis, 11-mm in each end of Y-axis. Since PMTs can only operate in a light tight environment, inevitably the detector enclosure further enlarges the dead region. In PEM studies, the overall peripheral nonsensitive area limits imaging near a patient's chest wall resulting in degrading diagnostic accuracy and efficiency.

One of the main challenges in PET instrumentation research and development is to achieve high spatial resolution, ideally in less than 2 mm. Even though PET cannot approach the fine resolution attainable from anatomy diagnosis instruments, such as X-ray radiography, CT and MRI, spatial resolution of 1 to 2 mm is still desirable in organ function studies [7].

In order to enlarge detector field of view, achieve higher spatial resolution, and reduce the detector peripheral dead region, we developed prototype modular detectors for our proposed PEM-II scanner.
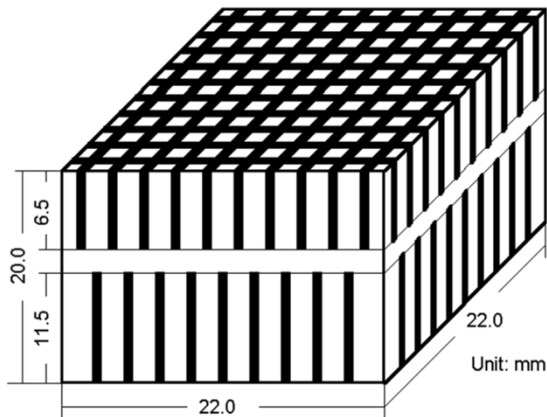
Fig. 1. This shows the structure and dimensions of BGO scintillation crystal for PEM-II detectors. The black regions in the graph demonstrate the saw-cut gaps.

Fig. 2. This is the diamond saw used for cutting BGO crystals. A crystal was held in the vice below the motor shaft and the diamond blades.

II. MATERIALS AND METHODS

We used Hamamatsu PS-PMT R7600-C12 [8] to build our new PEM-II detectors. R7600-C12 is a metal-channel type PMT fabricated with stacked thin electrodes. It has very narrow space between dynode stages and is constructed with a compact metal package instead of a traditional glass envelope. The package of PMT has outer dimensions of 26 mm × 26 mm, and the effective field-of-view is 22 mm × 22 mm.

A. Crystal Process

The solid BGO crystals we ordered [9] were 22 mm × 22 mm × 20 mm, with fine polished surfaces. We further prepared the crystals by cutting, chemical polishing, and epoxy encapsulating.

1) Crystal Pixelating: In PET detectors, block crystal designs with discrete or pseudodiscrete schemes have been extensively investigated and applied [10], [11]. We investigated a pseudodiscrete design in our previous PEM-I and ANIPET detectors [1]–[3]. The same BGO crystal pixelated scheme was applied in the new PEM-II detectors.

As depicted in Fig. 1, the crystal blocks were pixelated by diamond saw [12] into small elements of 1.98 mm × 1.98 mm (2.23-mm pitch) on two opposite faces. The elements on one face of the block are offset by half the crystal pitch from those on the opposite face in both X and Y axes. The crystal elements with 11.5-mm depth are coupled to the PS-PMT window—we describe this layer as the "near the PMT-window layer" or the "near-layer." Those with 6.5-mm depth are on the opposite face, described as the "far-layer." This crystal depth scale are based on a Monte Carlo simulation result ensuring an equal probability of gamma ray interaction in each of two layers [1]. With this scheme, one bit depth-of-interaction information can be obtained by identifying the layer in which events occur.

Fig. 2 shows the cutting diamond machine. Normally, three diamond blades (0.25-mm thickness) can be mounted on the shaft in a single cutting pass. The multiple blades were separated by 1.85-mm thick aluminum flanges. During the cutting operation, the blades rotating speed were adjusted to 1000 RPM. Due to the hardness and fragility of the BGO characteristics, the feed speed was set to the machine minimum value (about 0.05 mm/s).
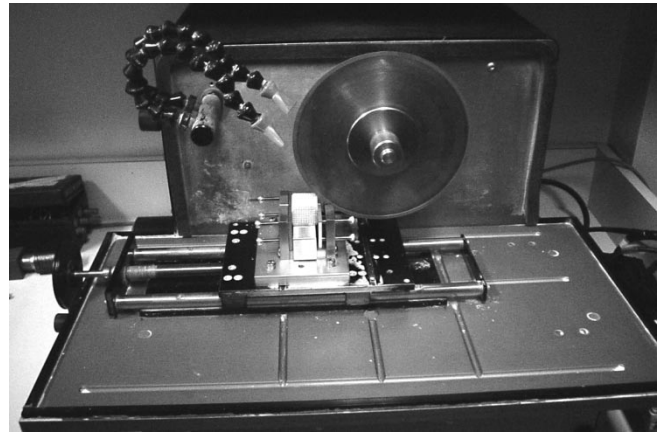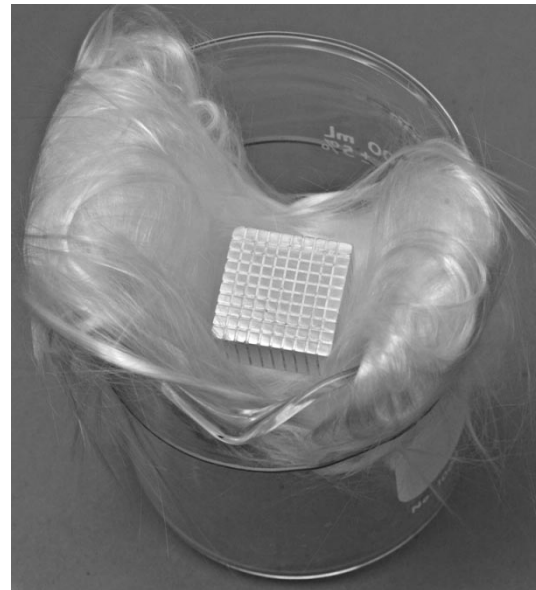

Fig. 3. A crystal block was sunk into the acid-etching bath and supported by glass wool cushion.

A specific coolant (containing rust-inhibitor) steadily streams over the crystal surface. The coolant prevents heat generation in the blades and the crystal—the heat expansion could break the crystal element.

2) Crystal Chemical Polishing: After we cut the crystals, the cut surfaces produced by diamond saw blades became very rough. This roughness would degrade the light collection [13]; therefore we need to polish the crystals. Since the cut crystals were extremely fragile, and the crystal elements are in the complex pattern, it is extremely difficult to polish the crystals mechanically. For that reason, chemical polish by acid etching was chosen to polish the surfaces of all the crystal elements.

The etching acid is a solution of 30% Hydrochloric (HCL) and 70% Nitric acid (HNO_3) [14]. The cut crystal was placed on a band of glass wool immersed in the solution for 5 min (Fig. 3). Then the beaker holding the solution was put in an ultrasound bath in another 2 min. Next, the crystal block was removed from acid and rinsed under a thin stream of water. Finally, it was rinsed again with ethanol solution. By carefully following these
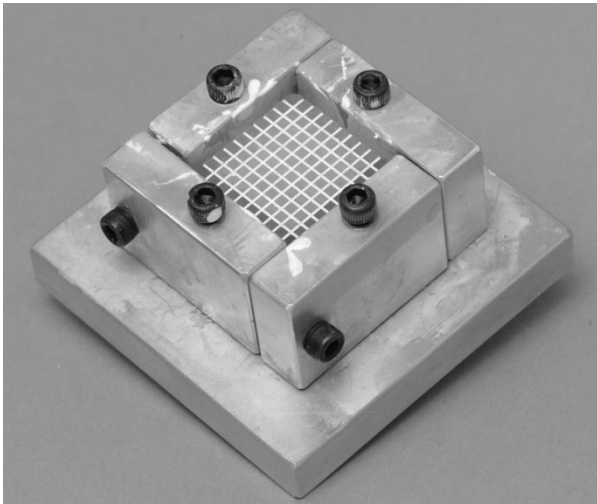
Fig. 4.   The inner dimensions of the mode are 23.00 mm × 23.00 mm × 21.00 mm, with a tolerance of ±0.05 mm.
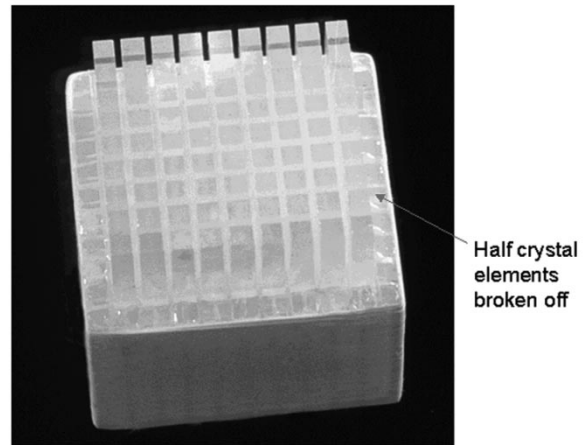

Fig. 5.   After cutting and acid polishing, the near-layer of the crystal block was encapsulated with epoxy compound and surrounded by white Teflon tape. The half-crystal elements of the far-layer in the image were already removed.
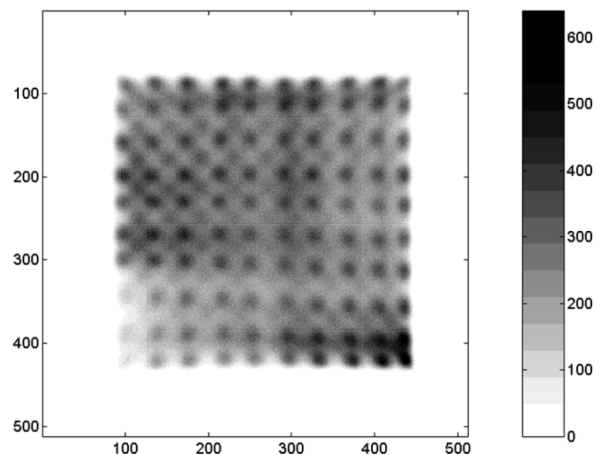

Fig. 6.   This is a BGO crystal front-flood irradiation image with a ^{68}Ge source. The hardware lower energy threshold is 150 keV.

steps, the risk of breaking the crystal elements off the block is sufficiently reduced.

3) Crystal Epoxy Encapsulating: The acid etching makes the crystals even more fragile, any additional mechanical processing (painting, packing) may easily break the crystal elements, so we chose encapsulating epoxy compound to coat crystal elements.

The criteria for selecting epoxy compound are that it is both optically opaque and high reflective. Optically opaque compounds can isolate light transmitted to adjacent crystal elements; high reflectivity will largely recover the light transmitted outside the event crystal volume. The reflectivity of the coating material is important because significant fraction of the scintillation light may interact with this reflector before finally reaching the PMT window [15].

The epoxy compound selected includes a two-component epoxy, and an epoxy base coloring paste. The epoxy product is "EPO-TEK 301-2" [16] containing base epoxy (part-A) and hardener (part-B) two components. Their mixed ratio is 100 to 35 parts by weight. Since the mixed epoxy is transparent after curing, we colored the epoxy mixture with an epoxy-based white paste (REN DW-0131). The proportion of white paste to epoxy was 2 to 1 parts by weight. The mixed product was opaque, highly reflective, and of relatively low viscosity.

The low viscosity compound was chose to fill the crystal cutting gaps without trapping air bubbles, but the tradeoff is that the compound could drain out of the gaps before curing. To solve this problem, an aluminum mold was built to confine the potting material. Fig. 4 shows the mechanical drawing of the potting mold. The four molding walls were fixed to the aluminum plate, and secured each other with screws after the crystal array is positioned. All the molding walls were designed for easy assembly and removal. The inner walls and the top surface of the plate were all polished.

The release agent RP 79-2 [17] was chosen to facilitate the release of the cured crystal from the aluminum-encapsulating mold. It is an aerosol, semi-permanent, and dry-file Teflon based release agent formulated without wax or silicone, designed es-

pecially for epoxy applications [18]. We sprayed a thin layer of the RP 79-2 agent to the inner surfaces of mold before encapsulating. The agent transferred the epoxy curing resist from the mold to the encapsulating crystal block.

4) Edge Crystals in the Far-Layers: After the cutting process, the solid crystal block has 10×10 elements in the near-layer, and $(1/2 + 9 + 1/2) \times (1/2 + 9 + 1/2)$ elements in the far-layer (Fig. 1). By evaluating the crystal irradiation images, we found that the edge crystal elements in the far-layer are not visible. Images show that these edge elements are even blurring the edge near-layer elements and the inner far-layer elements as well. Hence, we decided to break out entire far-layer edge crystal elements to reduce the image distortion. To avoid damaging the near-layer crystal elements, this procedure was done after encapsulating the near-layer. Fig. 5 shows a partially finished crystal. The near layer has been filled with reflector and the edge crystal elements have been removed from the far layer.

5) The Uncut Region Between the Near and Far Layers: Fig. 6 shows an initial crystal identification image resulting from frontal irradiation with a ^{68}Ge source [19]. In this image,
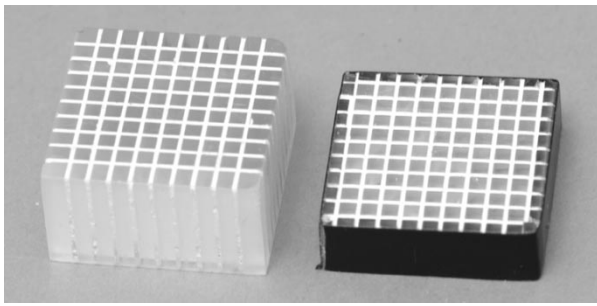
Fig. 7.   The crystal of 22 mm × 22 mm × 20 mm was cut into two segments. The interconnecting uncut region was eliminated.

the near-layer elements can be clearly identified. The far-layer elements can be accentuated by applying an energy-banding technique [19]. As shown in Fig. 6, there are near-far element overlaps in the images. These overlaps would cause difficulty in assessing the depth of interaction information.

We subsequently investigated other methods intended to better identify crystal elements in both layers [19]. The most successful approach was to completely eliminate the 2-mm uncut region interconnecting the near and far layers. Our Monte Carlo simulation also indicated that this uncut region could be a cause of the near-far image blurring [15].

We first cut the crystal along the uncut-region with a thick diamond saw blade (1-mm thickness). Fig. 7 shows the separated two layer segments. Next, we mechanically removed the remnants of uncut regions on both segments. Then we mirror-polished the cut surfaces providing a specular-reflective finishing. Finally, the two segments were aligned and glued together by an optical coupling compound—a product of Sylgard-186 [9] containing two components of Silicone Elastomer (part A) and hardening agent (part B). The mixed ratio is 10 parts elastomer to 1 part curing agent by weight. The index of refraction of Sylgard-186 is 1.465.

6) Optimizing the Crystal Process Procedure: The optimized crystal processing procedures are illustrated in Fig. 8 flowchart. Compared with the crystal operation procedures in PEM-I and ANIPET detectors, we added two major steps: crystal cutting along the interconnection uncut region and crystal segments etching. Even though the pixelated and acid-etching crystals were very fragile, they became quite solid after encapsulating with adhesive epoxy-pigment mixture. It turns out that the process of cutting along the uncut region is much easier than pixelating the near and far layers.

B. Front-End Electronic Circuits

The front-end electronics in our new detectors include crossed anode readout circuits, modified high-voltage dividers, position preamplifier circuits with voltage-feedback amplifiers, and timing preamplifier circuits with current-feedback amplifiers. We investigated a method of combining four PS-PMTs with simplified four (X^-, X^+, Y^-, and Y^+) outputs to further simplify the position processing [19].

Fig. 9 shows the PS-PMT socket with modified high-voltage divider and anode resistor chains. The signal from PMT last dynode is taken out from the socket for event timing. The position integrating and timing amplifying circuits stack are shown
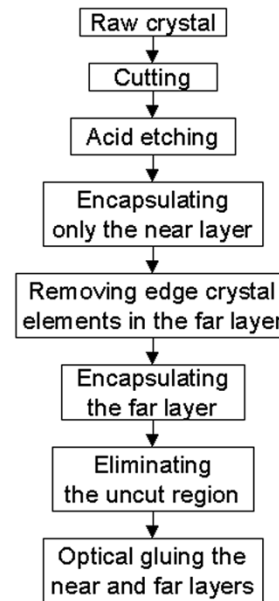

Fig. 8.   This flow-chart illustration the optimized procedure in crystal processing.
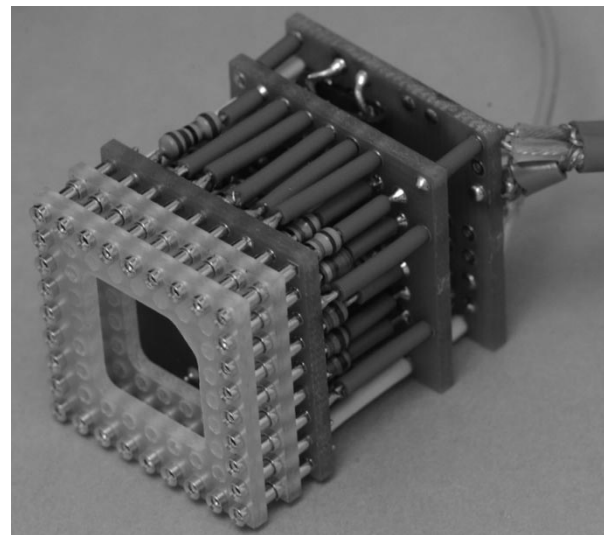

Fig. 9.   This shows the PMT socket with high-voltage divider and anode resistor chain circuits.

in Fig. 10. The printed circuit boards (PCBs) are miniature so they can fit in the detector enclosure.

C. Detector Array, Module, and Unit Configuration

The PEM-II system is constructed with two detector arrays; each one is divided into four modules; each module consists of four detector units; each unit has one dual-layer BGO crystal optically coupled to a PS-PMT. The basic detector unit is designed as "field-replaceable-unit." Each detector module has its own position and timing electronic circuits with (X^-, X^+, Y^-, and Y^+) and a timing trigger output. One module in a detector array can have coincidence with any module in the opposite detector array. The coincidence events in different module pairs can be processed simultaneously. Fig. 11 shows the detector array-module-unit structure.
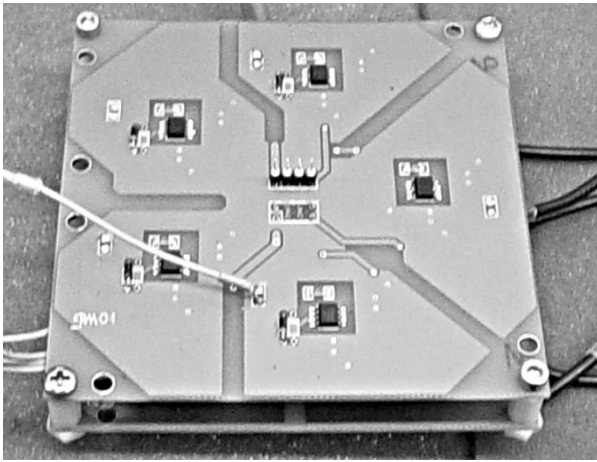
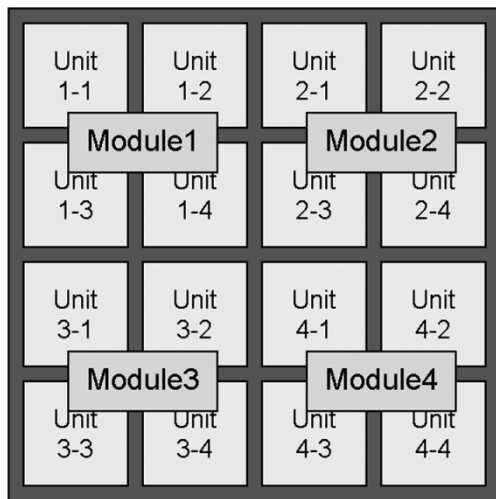Fig. 10. This is the stack of the front-end position integrator and the last dynode timing amplifier circuit.

Fig. 12. The crystal boundary fish-net overlaps on the crystal irradiation images.

Fig. 11. This is the configuration map of one detector array. Each array has four modules. Every module has four detector units.

Fig. 13. This crystal front-flood irradiation image. Crystal elements of 10 × 10 in the near-layer and 9 × 9 in the far-layer can be easily identified.

D. Distortion Look-Up-Table Generation

The distortion look-up-table was generated by MATLAB. Fig. 12 is the crystal identification "fish-net" array representing the boundary assignments for the crystal elements in both the near and far layers.

III. RESULTS

A. Front-Flood Irradiation Experiments

After eliminating the interconnecting uncut region, crystal irradiation images clearly shows the crystal elements in the near and far layers (Fig. 13). Compared with Fig. 6, the image overlaps between the near and far crystal elements were substantially reduced.

B. Coincidence Evaluations

The intrinsic spatial resolution was measured by pair detector units. Two point ^{68}Ge sources (0.78-mm diameter) were sepa-
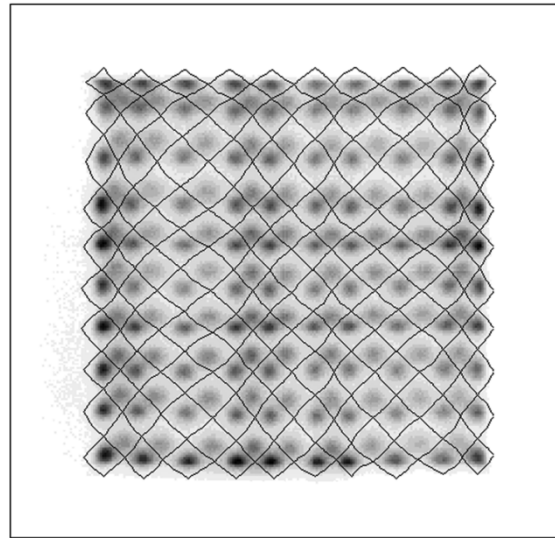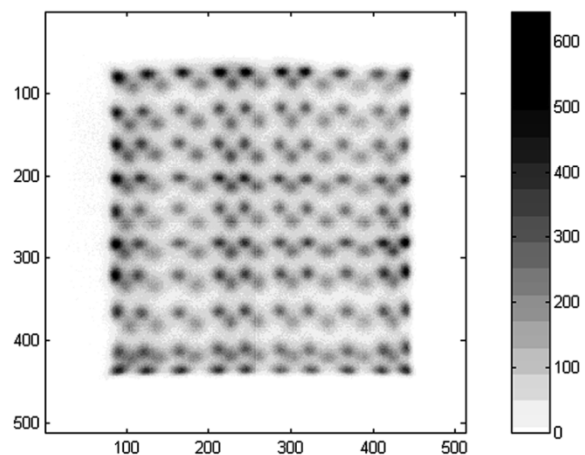
rated by 10 mm, placed in the center of faced detectors. Fig. 14 shows the coincidence results. The spatial resolution which is calculated from the full width of half maximum (FWHM) of Guassian fitting is 1.8 mm.

IV. DISCUSSION

Crystal processing is one of the crucial procedures in PET detector development. Multi-layer crystal designs have been investigated by many groups [20]–[22]. Most of them construct multi-layer crystals by gluing individual crystal elements to form a large, discrete crystal array. We pixelate the crystal from cutting a relatively large block into a dual-layer pseudodiscrete pattern. After acid etching and epoxy encapsulating, we cut the crystal into two separated layers. By polishing and gluing them together, we obtain a discrete dual-layer crystal array. This process turns out to be a time-efficient and cost-effective crystal making procedure.
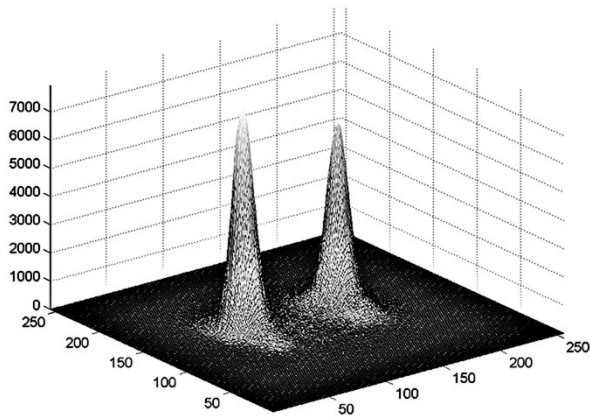
Fig. 14. This is coincidence experiment result acquired from two point ^{68}Ge sources (0.78-mm diameter). The result is demonstrated by using MATLAB mesh-display function.

ACKNOWLEDGMENT

The authors would like to thank D. Togane from the Centre for Addiction and Mental Health, University of Toronto, ON, Canada, E. del Campo from the Mechanical Workshop, Physics Department, McGill University, Montreal, QC, Canada, and Dr. S. Mzengeza from the Medical Cyclotron Facility, Montreal Neurological Institute for their technical assistants and supports. They would also like to thank Dr. W.-H. Wong from the University of Texas, M. D. Anderson Cancer Center, Dr. M. Kasahare from Hamamatsu Corporation, Bridgewater, NJ, and M. J. Hodgin from Epoxy Technology Inc., Billerica, MA, for many helpful discussions.

REFERENCES

[1] C. J. Thompson, K. Murthy, Y. Picard, I. N. Weinberg, and R. Mako, "Positron emission mammography (PEM): A promising technique for detecting breast cancer," *IEEE Trans. Nucl. Sci.*, vol. 42, pp. 1012–1017, Aug. 1995.

[2] C. J. Thompson, K. Murthy, I. N. Weinberg, and R. Mako, "Feasibility study for positron emission mammography," *Med. Phys.*, vol. 21, no. 4, pp. 529–538, 1995.

[3] C. J. Thompson, P. Sciascia, K. Murthy, S. Kecani, L. Nikinnen, E. Campo, J.-F. Corbett, Y. Bercier, M. Diksic, and P. Cumming, "ANIPET: a versatile PET scanner for imaging small animals," in *Proc. IEEE Nuclear Science Symp. Conf. Rec.*, vol. 2, Nov. 1998, pp. 1264–1267.

[4] "Hamamatsu catalog," in *Position-Sensitive Photomultiplier Tube, Type-R3941 Tech. Inform.*. Shimokanzo, Japan: Hamamatsu Photonics K. K., 1996.

[5] N. Zhang, C. J. Thompson, C. L. Thompson, and K. Q. Nguyen, "Improving the performance of small planar detectors for dedicated PET instruments," *IEEE Trans. Nucl. Sci.*, vol. 49, pp. 111–115, Feb. 2002.

[6] R. L. Clancy, C. J. Thompson, J. L. Robar, and A. M. Bergman, "A simple technique to increase the linearity and field-of-view in position sensitive photomultiplier tubes," *IEEE Trans. Nucl. Sci.*, vol. 44, pp. 494–498, June 1997.

[7] S. R. Cherry, Y. Shao, R. W. Silverman, K. Meadors, S. Siegel, A. Chatziioannou, J. W. Young, W. Jones, J. C. Moyers, D. Newport, A. Boutefnouchet, T. H. Farquhar, M. Andreaco, M. J. Paulus, D. M. Binkley, R. Nutt, and M. E. Phelps, "MicroPET: A high resolution PET scanner for imaging small animals," *IEEE Trans. Nucl. Sci.*, vol. 44, pp. 1161–1166, June 1997.

[8] "Hamamatsu catalog," in *Position Sensitive Photomultiplier Tube R7600-00-C12 Preliminary Data.*. Shimokanzo, Japan: Hamamatsu Photonics K. K., October 1998.

[9] Alpha Spectra, Inc., , Grand Junction, CO.

[10] M. P. Tornai, G. Germano, and E. J. Hoffman, "Positioning and Energy response of PET block detectors with different light sharing schemes," *IEEE Trans. on Nucl. Sci.*, vol. 41, pp. 1458–1463, Aug. 1993.

[11] W.-H. Wong, "A positron camera detector design with cross-coupled scintillators and quadrant sharing photomultipliers," *IEEE Trans. Nucl. Sci.*, vol. 40, pp. 962–966, Aug. 1993.

[12] South Bay Technology Inc., San Clemente, CA.

[13] J. L. Robar, C. J. Thompson, K. Murthy, R. L. Clancy, and A. M. Bergman, "Correction of spatial distortion, gain nonuniformity and efficiency variation in detectors for positron emission mammography," *IEEE Trans. Nucl., Sci.*, vol. 44, pp. 1206–1210, 1997.

[14] J. L. Robar, "Construction and calibration of detectors for high-resolution metabolic breast cancer imaging," M. Sc. thesis, McGill University, Montreal, QC, Canada, Aug. 1996.

[15] F. Cayouette, C. Moisan, N. Zhang, and C. J. Thompson, "Monte carlo modeling of scintillator crystal performance for stratified pet detectors with DETECT2000," *IEEE Trans. Nucl., Sci.*, vol. 49, pp. 624–628, June 2002.

[16] Epoxy Technology Inc., , Billerica, MA.

[17] Vantico Inc., "Ren shape tooling systems,", East Lansing, MI.

[18] "Ren tooling epoxy resin systems," in *Ren Tooling Epoxy Selector Guide—Technical Document*. East Lansing, MI: Ren Shape Tooling Syst..

[19] N. Zhang, C. J. Thompson, D. Togane, F. Cayouette, and K. Q. Nguyen, "Anode position and last dynode timing circuits for dual-layer BGO scintillator with PS-PMT based modular PET detectors," *IEEE Trans. Nucl. Sci.*, vol. 49, pp. 2203–2207, Oct. 2002.

[20] T. Yamashita, M. Watanabe, K. Shimizu, and H. Uchida, "High resolution block detectors for PET," *IEEE Trans Nucl. Sci.*, vol. 37, pp. 589–593, 1990.

[21] J. Seidel, J. J. Vaquero, S. Siegel, W. R. Gandler, and M. V. Green, "Depth identification accuracy of a three layer phoswich PET detector module," *IEEE Trans. Nucl. Sci.*, vol. 46, pp. 485–490, June 1999.

[22] J. J. Vaquero, J. Seidel, S. Siegel, and W. R. Gandler, "Performance characteristics of a compact position-sensitive LSO detector module," *IEEE Trans. Nucl. Sci.*, vol. 17, pp. 967–978, Dec. 1998.